Characteristics of Winter Precipitation Variation over Northern Central Eurasia and Their Connections to Sea Surface Temperatures over the Atlantic and Pacific Oceans

HENGCHUN YE

Department of Geography, University of Idaho, Moscow, Idaho

(Manuscript received 8 June 2000, in final form 22 January 2001)

ABSTRACT

This study reveals spatial and temporal characteristics of precipitation variability and their teleconnections to sea surface temperatures (SSTs) over the Atlantic and Pacific Oceans by analyzing 68 yr of recent precipitation records over the former Soviet Union. In addition to a general increasing trend of about 0.4 mm yr^{-1} or 6% $decade^{-1}$ over much of the study region, three major modes of precipitation variation are identified. A quasi-biennial variation of 2–3 yr is found over the region surrounding the Caspian and Aral Seas. An El Niño timescale precipitation variation of 4–5 yr is present over southern central Siberia and is associated with eastern tropical Pacific SSTs. A quasi-decadal timescale variation of about 11–12 yr is evident over central European Russia. This quasi-decadal precipitation variation is closely linked to a major SST anomaly pattern of alternating latitudinal belts over the Atlantic and SST variations over the equatorial Pacific Ocean. These associations to SSTs are stronger at the timescales identified in this study than at an interannual timescale.

The atmospheric west Atlantic pattern and atmospheric anomalies over the eastern tropical Pacific bridge the teleconnection between precipitation over central European Russia and both oceans at quasi-decadal timescales. The atmospheric anomalies over the eastern Pacific coupled with eastern tropical SST anomalies are teleconnected to those over northern Asia and, thus, are responsible for the precipitation variation over southern central Siberia at an El Niño timescale.

1. Introduction

Evidence emerging from studies of climate variation and change strongly suggest that the climate system exhibits quasi-periodical variations at various timescales in addition to trends that are suspected to be of anthropogenic origin. Biennial and El Niño timescale variations have been found in many surface climate parameters as well as in atmospheric circulation (Dettinger et al. 1995; Lall and Mann 1995; Mann and Park 1994; Reed et al. 1961; Ropelewski and Helpert 1987; Sathiyamoorthy and Mohanakumar 2000; Shen and Lau 1995; Veryard and Ebdon 1961; Trenberth and Olson 1988). Decadal timescale variations are also found in many regions of the world (Table 1). These include temperature, precipitation, river streamflows, lake water volume, and snow depth over North America and Eurasia (Cook et al. 1997; Currie and O'Brien 1992; Dettinger et al. 1995; Eischeid et al. 1985; Guetter and Georgakakos 1993; Haston and Michaelson 1994; Lall and Mann 1995; Latif and Barnett 1996; Liang et al. 1995; Livezey and Smith 1999; Mann et al. 1995; Mann and Park 1994; Yatagai and Yasunari 1994; Ye 2000). These studies suggest that quasi-decadal variations are associated with the Atlantic Ocean while interdecadal variation is of Pacific origin. Direct connections between surface climates and SSTs at decadal timescales are revealed in some of the above studies.

A better understanding of the teleconnections between SST anomalies and land surface climates (Bitz and Battisti 1999; Folland et al. 1986; Gershunov et al. 1999; Jakowski et al. 2000; Livezey and Smith 1999; Peng and Mysak 1993; Ropelewski and Helpert 1987; Ting and Wang 1997; Wallace et al. 1995; Ye 2000) promises improved predictability of surface climate (Barnston and Smith 1996). In addition to El Niño, SST anomalies over the northern Pacific and Atlantic Oceans also have widespread associations with surface climate. For example, low-frequency SST variations over the western tropical and northern Pacific Ocean have a significant impact on surface climates over some mid- and high-latitude regions (e.g., Bitz and Battisti 1999; Gershunov et al. 1999; Jakowski et al. 2000; Ting and Wang 1997). Atlantic sea surface temperature anomalies and the associated atmospheric North Atlantic oscillation (NAO) are closely related to surface climate variations over Eurasia (Hurrell 1995, 1996; Hurrell and van Loon 1997; Mann and Park 1996; Moses et al. 1987; Peng and Mysak 1993; Rogers 1997; Ye 2000; Wallace et al. 1995). It is likely that persistent atmospheric circulation anomalies coupled with oceans exert their influence on

Corresponding author address: Dr. Hengchun Ye, Department of Geography, University of Idaho, Moscow, ID 83843.
E-mail: yehe@uidaho.edu

TABLE 1. Summary of studies that revealed decadal variations in surface climate parameters.

Geographic regions	Variables	Timescales	Authors
Global	Air temperature	Quasi-decadal of 7–8 yr and 11–12 yr Interdecadal of 15–18 yr	Mann and Park (1994)
North America	Air temperature	Interdecadal	Livezey and Smith (1999)
North America	Air temperature and precipitation	Quasi-decadal	Latif and Barnett (1996)*
United States	Air temperature and precipitation	Quasi-decadal	Mann et al. (1995)
United States	Air temperature	Quasi-decadal of about 10 yr Interdecadal of about 25 yr	Dettinger et al. (1995)
United States	Streamflow	Quasi-decadal	Guetter and Georgakakos (1993)
United States	Precipitation	Quasi-decadal of 10–11 yr Interdecadal of 17–20 yr	Currie and O'Brien (1992)
Western United States	Drought index	Bidecadal of about 22 yr	Cook et al. (1997)
California	Precipitation	Interdecadal of about 20 yr	Haston and Michaelson (1994)
Great Salt Lake Basin	Precipitation	Quasi-decadal	Eischeid et al. (1985)
Great Salt Lake	Lake water volume	Quasi-decadal and interdecadal	Lall and Mann (1995); Mann et al. (1995)
China	Winter temperature summer precipitation	Decadal	Yatagai and Yasunari (1994)
East China	Monsoon rainfall	Interdecadal of 21, 30, and 47 yr	Liang et al. (1995)**
Russia	Winter snow depth	Quasi-decadal of 11.8 yr and interdecadal of 20 yr	Ye (2000)

* Combination of coupled models and observations.
** GCM model simulated study.

distant land surface climates through atmospheric teleconnectivity.

Along with the quasi-biennial and 4–7-yr variations associated with El Niño (e.g., Dickey et al. 1992; Keppenne and Ghil 1992), decadal variation is an important characteristic of SST variability. A major SST variation pattern over the North Atlantic that is associated with the NAO fluctuates at a quasi-decadal timescale (Desser and Blackmon 1993; Häkkinen 2000; Kushnir 1994; Latif and Barnett 1996; Mann and Park 1996; Reverdin et al. 1997; Xie and Tanimoto 1998). The decadal variation of SSTs over the Pacific Ocean is most significant in extratropical and western tropical Pacific regions (Latif et al. 1997; Namias et al. 1988; Pierce et al. 2000; Yamagata and Masumoto 1992; Zhang et al. 1997). Few studies have investigated the potential teleconnections between SSTs and surface climate parameters at these quasi-periodic timescales.

Trends in precipitation over high-latitude regions have been revealed in many studies (Bradley et al. 1987; Brown 2000; Dai et al. 1997; Groisman and Easterling 1994; Fallot et al. 1997; Ye et al. 1998; Wang and Cho 1997). Part of these trends may be associated with decadal-and-longer timescale low-frequency sea surface temperature (SST) variations like similar trends in surface air temperature (Hurrell 1995; Livezey and Smith 1999; Mann and Park 1996; Wallace et al. 1995). Although quasi-biennial and El Niño timescale variations in precipitation over northern Eurasia have been identified (Wang and Cho 1997), decadal variability, which may parallel variability in SSTs, has not been examined. In addition, the teleconnections of these quasi-periodical variations in precipitation and SSTs deserve investigation to better understand the variability and predictability of land surface precipitation over high-latitude land areas.

The goal of this study is to investigate the spatial patterns and temporal characteristics of winter precipitation variation over northern-central Eurasia and their connections to SSTs over the Atlantic and Pacific Oceans. More specifically, the author aims to identify the geographic regions and quantify the dominant timescales of the teleconnections, and to reveal the associated atmospheric circulation patterns that bridge the connections by applying advanced statistical methods to 68 yr of data.

The paper is organized as follows. Section 2 consists of data descriptions (section 2a) and statistical methods (section 2b). Section 3 presents results including precipitation variation characteristics (section 3a), associations to the Atlantic Ocean (section 3b), Pacific Ocean (section 3c), and the atmospheric anomaly patterns associated with the teleconnections (section 3d). Section 4 is a summary of the findings and discussions.

2. Data and methodology

a. Data

Precipitation data are derived from the former Soviet Union Monthly Precipitation Archive, 1891–1993, available from the National Snow and Ice Data Center, Boulder Colorado. This dataset has been quality controlled and corrections have been made to justify for

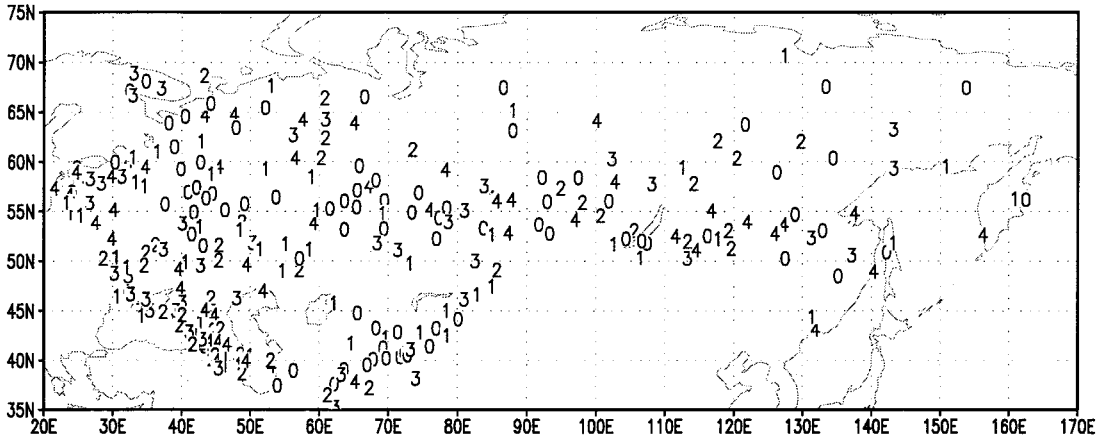

FIG. 1. Station locations and the number of missing winters during 1926–93.

observation time and rain gauge changes, as well as wind and wetting losses using methods developed by Groisman et al. (1991). If only one month in a winter season (Dec–Jan–Feb) is missing, it is interpolated from the month before and the month after. If more than one month is missing, the entire season is considered as missing. Thus, 261 out of 622 original stations (each of which has less than 5 missing winters during the time period of 1926–93) are selected for this study. Among these 261 stations, 73 stations have 1 interpolated month, 52 stations have 2, 33 stations have 3, and 5 stations have 4 or more. A large fraction of these interpolated months fall in the first and last 2 yr of the study period. Considering the small number of months interpolated, the method of interpolation has little influence on the general results. The station distribution is shown in Fig. 1. A reasonably good density of station distribution is found over western Russia and southern-central and eastern Siberia.

Total winter precipitation for each station is then interpolated into grid points of size 5° latitude by 2.5° longitude using Shepard's local-search interpolation on a spherical surface formulated by Willmott et al. (1985). The interpolation is performed for each winter. Stations that have missing seasonal precipitation are not used in the interpolation for that particular winter. Based on station distribution, some grid points are too far away from nearby stations to have reliable values. Grid points that have at least one missing value during the study time period are excluded from the study. As a result, a total of 212 grid points covering European Russia, western Siberia, southern-central Siberia, and southeastern Siberia are selected for further analyses (Fig. 2).

The distribution of mean total winter precipitation is displayed in Fig. 3. Total winter precipitation (Dec–Jan–Feb) ranges from 5 to 10 cm in much of the study region. Precipitation over European Russia is slightly higher: 10–15 cm. Winter precipitation decreases toward the east, with Siberia only receiving about 5 cm each winter. A small wet region with precipitation as high as 40 cm is located east of the Black Sea, in Georgia, due to lake effect snowfall and the orographic effect of the Caucasus Mountains. Total winter precipitation at each grid point is standardized before statistical analyses.

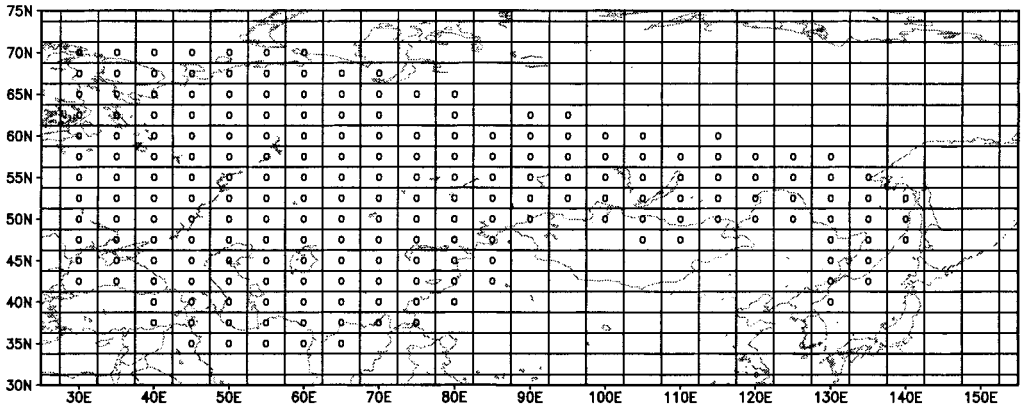

FIG. 2. Gridpoint distribution. Grid points with ''o'' have no missing values during the entire study time period and are used in analyses.

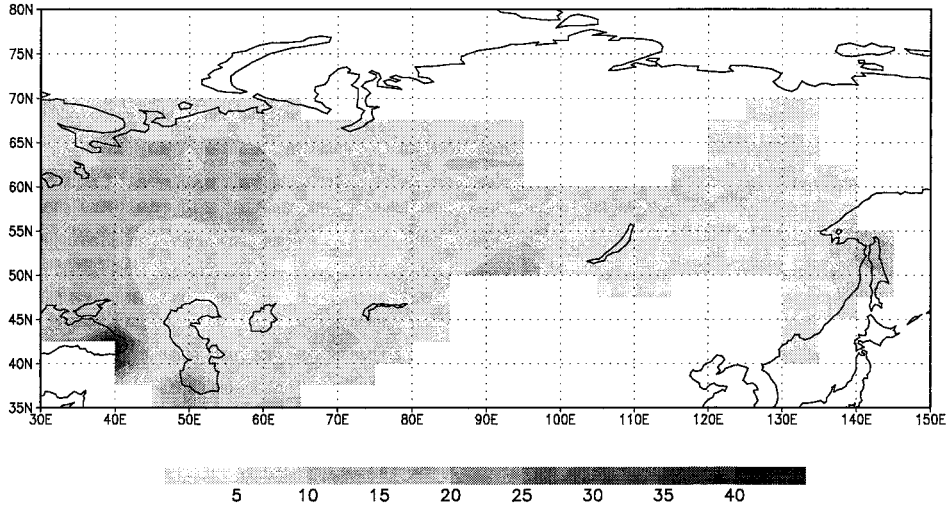

FIG. 3. Mean total 3-month winter precipitation (cm) during 1926–93.

The SST data are derived from the gridded monthly Global Sea-Ice and SST dataset (GISST, version 2.3b) compiled by the Hadley Centre for Climate Prediction and Research Meteorological Office. This dataset is chosen because of its long record length. The time period overlapping the precipitation data is selected. These SST data have a resolution of 1° latitude by 1° longitude and are quality controlled (Folland and Parker 1995; Parker et al. 1995). Four different methods have been used in constructing the SSTs of GISST for the four time periods of 1903–48, 1949–81, 1982 to the present, and an extension of 1903 back to 1871. Details of the reconstruction methods are summarized by Hurrell and Trenberth (1999).

The Reynolds Reconstruction of the Comprehensive Ocean–Atmosphere Data Set (COADS) SST data covering the time period of 1950–92 (Smith et al. 1996) are also used. SST anomalies in this dataset were reconstructed based on the dominant empirical orthogonal function modes derived from the more recent period of 1982–93. The reconstruction method used in this dataset produces more realistic large-scale SST structures in sparsely sampled regions than traditional analytical techniques, and is thought to be of better quality than GISST for the time period after 1981 (Hurrell and Trenberth 1999). This COADS's SST dataset has a resolution of 2° latitude by 2° longitude. It is used to duplicate analysis for the more recent time period (1951–92) and to test the robustness of the teleconnection patterns in SSTs derived from different reconstruction methods. Grid points over both the Atlantic and Pacific Oceans between 20°S and 70°N are selected for this study. The cutoff at 20°S is designed to avoid unreliable seasonal mean SSTs caused by the low density of observations south of 20°S (Hurrell and Trenberth 1999). The mean winter SSTs are the averages of the 3-month mean SSTs of December, January, and February.

Monthly mean 700-mb height data are taken from the National Centers for Environmental Prediction–National Center for Atmospheric Prediction's reanalysis products (Kalnay et al. 1996) covering the time period 1950–93. The grid points are 2.5° latitude by 2.5° longitude and those distributed over the entire Northern Hemisphere are selected. The mean winter geopotential heights are the averages of the same 3-month means as those of precipitation and SSTs.

b. Statistical methods

First, rotated principal component analysis is used to reduce the data dimension and define major spatial variation patterns of winter precipitation over northern-central Eurasia. Then, singular spectrum analysis (SSA) is applied to each rotated principal component (RPC) associated with the retained variation patterns (rotated eigenmodes or REOFs) to reveal and extract any periodical behaviors or oscillations. Cross-correlation maps showing the distribution of correlation coefficients between each RPC and time series of SSTs at grid points over both the Atlantic and Pacific Oceans are produced to define the geographic regions over the oceans where statistically significant correlations are present.

SSA is a powerful tool for time series analysis that can identify intermittent oscillation spells in short, noise time series (Vautard et al. 1992). Mathematically, it is similar to PCA but reveals temporal variation patterns of a single time series using a predefined window length (or the maximum lag in the correlation matrix). The basic oscillations into which a time series decomposes are not functions of prescribed, harmonic form. Instead, their shapes are determined from the time series itself. SSA has been successfully used in many geophysical and climatological studies to reveal and predict periodic activities (e.g., Ghil and Mo 1991; Ghil and Vautard 1991; Plaut and Vautard 1994; Wang and Cho 1997; Ye 2000; Zhang et al. 1998). A complete discussion of the

technique is found in Elsner and Tsonis (1996) as well as Vautard et al. (1992).

Eigenvalues produced from SSA using Vautard and Ghil's (1989) algorithm in computing the covariance matrix are sorted in descending order. The two nearby eigenvalues form a pair if they are nearly equal and together they potentially represent an oscillation component. The frequency of the oscillation pair is determined by the power spectra of the corresponding temporal principal components (T-PCs) using maximum entropy method (Barrodale and Erickson 1980). The criteria for selecting an oscillation pair are 1) the frequencies f_k and f_{k+1}, corresponding to the maximum spectral values of the kth T-PC (T-PC$_k$) and the $k + 1$th T-PC (T-PC$_{k+1}$) satisfies $2M|f_k - f_{k+1}| < 0.75$ (with M as the window length); and 2) the lags at which cross correlations between T-PC$_k$ and T-PC$_{k+1}$ are maximized and statistically significant at approximately one-quarter of the oscillation period.

The time evolution of each identified oscillation component is extracted from the original time series to produce a reconstructed oscillation component (RC). Please refer to Plaut and Vautard (1994) and Vautard et al. (1992) for details of the reconstruction technique. In this study, Vautard et al.'s (1992) algorithm is used in the reconstruction.

The RCs are also correlated to SSTs of both the Atlantic and Pacific Oceans to compare the relative significance of the connections at the oscillation timescales versus the interannual timescale derived from the RPCs. In addition, any lag relationships between precipitation and SSTs are explored using cross-correlation maps with various lags.

Cross-correlation coefficient maps depicting the correlation coefficients between each RPC and time series of winter 700-mb heights at grid points over the Northern Hemisphere are produced to show atmospheric circulation anomalies. The RCs are also correlated to geopotential heights to further reveal the atmospheric anomaly patterns associated with oscillatory behaviors.

In determining the statistically significant correlation areas in cross-correlation maps, the autocorrelation of the RPC (or RC) and the time series of SSTs (or 700-mb heights) at grid points are adjusted by defining the equivalent sample size for the correlation field. The definition of equivalent sample size depends upon the parameter that is being tested and the way in which information is measured. In this study, the equivalent sample size is the actual sample size divided by the decorrelation time (t) (von Storch and Navarra 1999; von Storch and Zwiers 1999). The decorrelation time for the correlation between the RPC (or RC) and the time series of SSTs (or 700-mb heights) at each grid point is determined by

$$t = 1 + 2\sum_{k=1}^{n-1}\left(1 - \frac{k}{n}\right)\rho_x(k)\rho_y(k),$$

where $\rho_x(k)$ and $\rho_y(k)$ are the autocorrelation function of RPC (or RC) and SST (or 700-mb height) at lag k, respectively (von Storch and Zwiers 1999; von Storch and Navarra 1999),

$$\rho_x(k) = \frac{1}{\sigma^2}\,\mathrm{cov}(x_i, x_{i+k}), \qquad \rho_y(k) = \frac{1}{\sigma^2}\,\mathrm{cov}(y_i, y_{i+k}).$$

The first-order autocorrelation approximation AR(1) is used for both fields.

In addition, the degree of freedom adjusting for the spatial correlation of either SSTs or 700-mb geopotential heights is required for the test of field significance. This is done by adopting Chen's (1982) and Livezey and Chen's (1983) Monte Carlo simulation. One thousand random noise time series (normal distribution with zero mean and unit standard deviation) are generated and correlated to time series of SSTs (or 700-mb heights) at grid points to estimate the rejection rate of the statistically significant (at a 95% confidence level) correlation areas (in percentage). The rejection rate is the critical value of area percentage (ranked 50th highest out of the 1000 simulation outcomes) that must be exceeded in order to have a field significant at a 95% confidence level.

Before revealing any spatial and temporal variability in precipitation, the geographical distribution and the magnitude of trends in precipitation are examined. A linear least squares regression is developed for each grid point of the winter total precipitation over the 68-yr study time period. Due to possible autocorrelation in the precipitation time series, the equivalent sample size for each grid is smaller than 68. The decorrelation time (t) for each grid point of precipitation is estimated by

$$t = 1 + 2\sum_{k=1}^{n-1}\left(1 - \frac{k}{n}\right)\rho(k),$$

where $\rho(k)$ is the autocorrelation function at lag k and the AR(1) approximation is used. The resulting t ranges from 1.2 to 3 suggesting that the equivalent sample size for the precipitation time series at grid points ranges from 33 to 67.

The slopes of the regression line at grid points indicating the annual rate of change are plotted in Fig. 4a. Statistically significant areas adjusted for autocorrelation of the gridpoint time series are shaded. Significant trends are found in much of the study region with higher increasing rates over the western part of the study region where an increase of about 0.4 mm yr^{-1} is common. The percentage of precipitation increase for each grid point is estimated after dividing the annual change rate by the mean total winter precipitation of the grid. In general, precipitation has increased at about 6% decade^{-1} over much of northern-central Eurasia during the past seven decades (Fig. 4b).

Finally, to evaluate the field significance of the trends, the actual spatial degree of freedom due to the spatial correlation among grid points of precipitation needs to

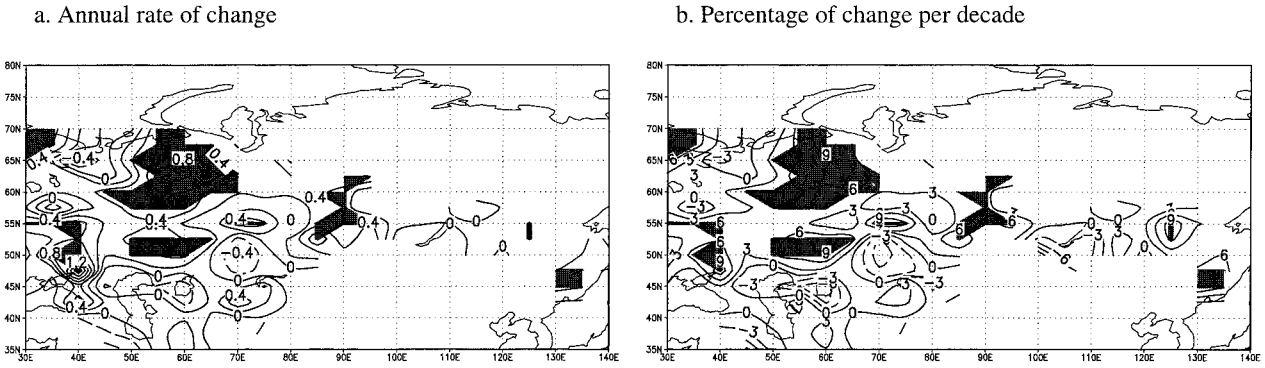

FIG. 4. The spatial distribution of precipitation trends during 1926–93 of (a) annual rate of change (mm yr^{-1} with a contour interval of 0.2), and (b) percentage of change per decade (% $decade^{-1}$ with a contour interval of 3). Shaded areas are statistically significant at a 95% confidence level based on the adjusted sample sizes for autocorrelation. Negative values are depicted with dashed lines.

be estimated (Chen 1982; Livezey and Chen 1983). Fraedrich et al.'s (1995) effective degree of freedom (DOF) formula is used for the precipitation field:

$$\text{DOF} = N^2 \Big/ \sum_{i=1}^{i=N} \lambda_i^2,$$

where λ_i is the ith eigenvalue of the cross-correlation matrix of precipitation at the N grid points. This equation is based on the assumption of a normal distribution of data. Square root transformation of the gridpoint precipitation is made before calculating the correlation matrix to satisfy a normal distribution assumption. As a result, the estimated degree of freedom is 14.3. Based on the probability of binomial distribution for 14.3 independent tests, 18.7% or more must pass the test to guarantee at least a 95% confidence level. The calculated significant trend area in which autocorrelation has been adjusted and grid points are weighted by the cosine of the latitude is 25.9%, which is greater than the rejection rate of 18.7%. This suggests that the trend in precipitation is field significant at above 95% confidence level.

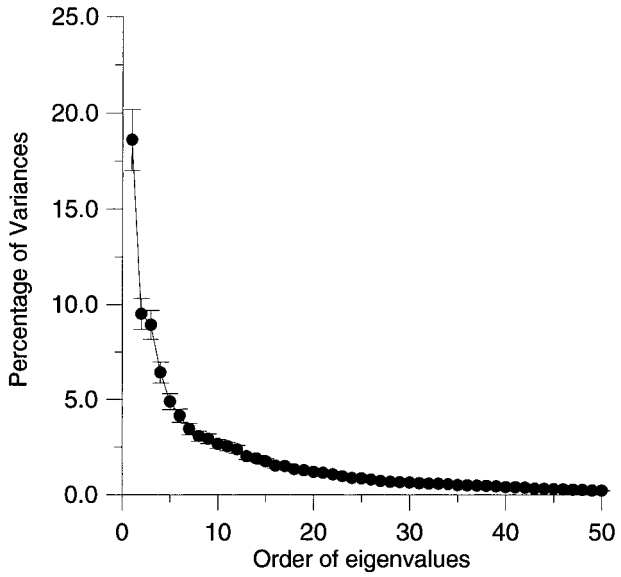

FIG. 5. Eigenvalues (in percentage) from PCA on precipitation and error bars indicating 95% confidence intervals.

3. Results

a. Precipitation variation characteristics

Since the grids span from 35° to 70°N, different grid surface areas are adjusted in principal component analysis (PCA) by a weighting coefficient of the square root of the cosine of latitude (Wallace et al. 1992). The first six major precipitation variation patterns produced by weighted PCA on standardized winter precipitation grids are retained for further analyses. These six principal components (PCs) are selected based on a statistically significant break (at a 95% confidence level) between the sixth and seventh eigenvalues according to North et al.'s (1982) formulation. The first 50 eigenvalues and 95% confidence error bars are plotted in Fig. 5. The eigenvalue plot suggests that these first six PCs are statistically significantly separated from each other at a 95% confidence level except PC2 and PC3 where possible overlapping between the two occurs. Together, these first six PCs explain 49.1% of the total interannual variance of winter precipitation.

These six PCs are used for rotation (VARIMAX method) to provide robust and more physically meaningful spatial patterns (Richman 1986, 1987). The spatial distribution patterns (REOFs) of the final six RPCs presented as the correlation coefficients between the corresponding RPC and the precipitation at grid points are mapped in Fig. 6. The first REOF (REOF1) describes precipitation variation over northern European Russia (Fig. 6a). The second REOF (REOF2) represents precipitation variation over central European Russia and southeastern Siberia (Fig. 6b). The third REOF (REOF3) emphasizes precipitation variation over southern European Russia, an area around and east of the

TABLE 2. Trends and oscillatory components of winter precipitation over northern-central Eurasia identified by SSA with a window length of 13. All the correlations are statistically significant at the 99% confidence level or above. Lags are positive when T-PC$_k$ leads T-PC$_{k+1}$, and negative otherwise.

RPCs	Components (orders of T-EOFs/ T-PCs)	Periods (yr)	Variance explained	Maximum lag cross correlations between oscillatory pair of T-PCs
RPC2	1	Trend	22.5%	0.909 at lag 3
	2–3	11.8 yr	27.6%	−0.919 at lag −3
RPC3	1	Decadal	13.3%	0.521 at lag 1
	6–7	2.5 yr	16.6%	−0.530 at lag −1
RPC4	1	Interdecadal	29.3%	0.514 at lag 1
	2–3	4.75 yr	18.5%	−0.485 at lag −1

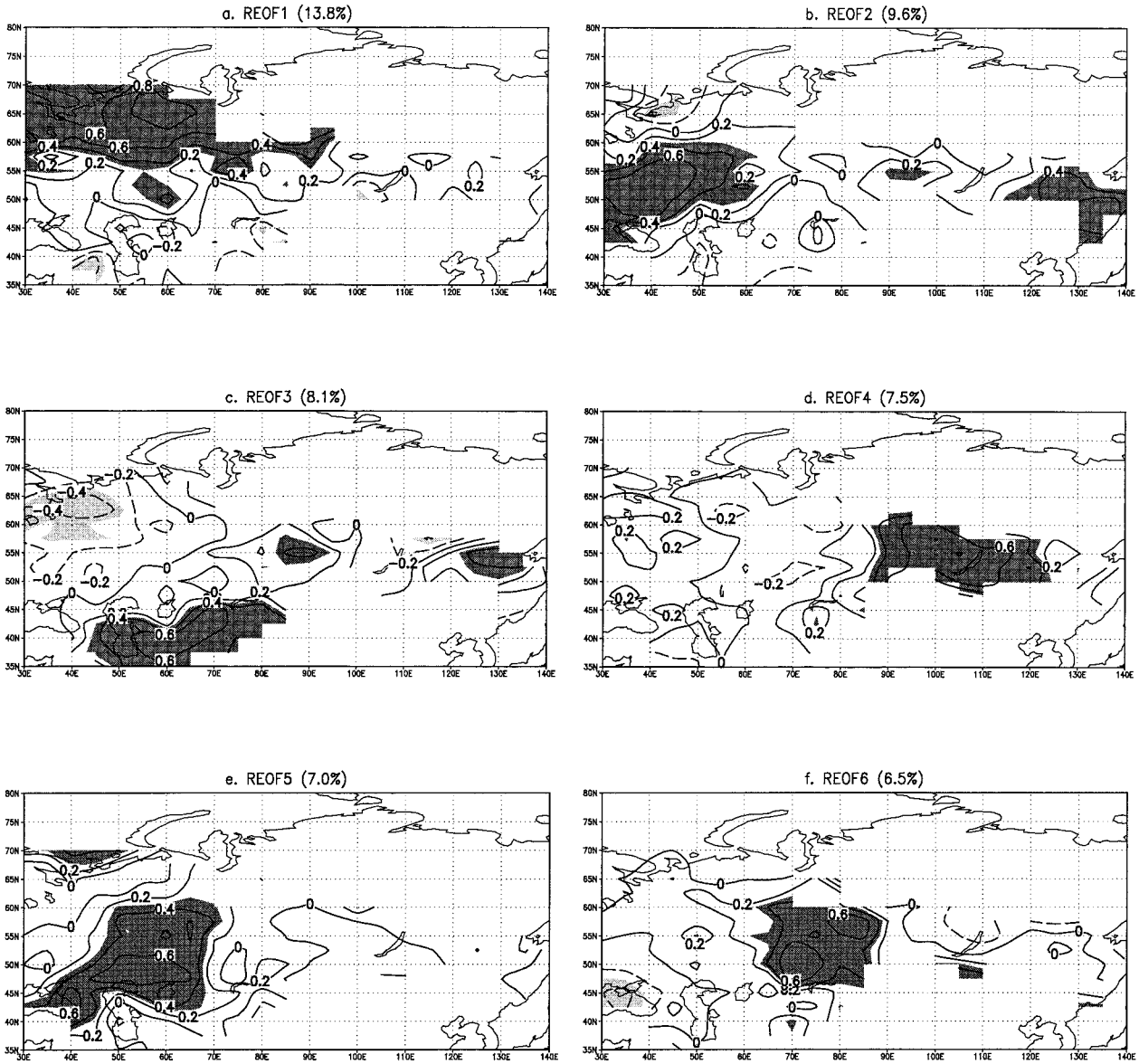

FIG. 6. Six REOFs represented by the correlation coefficients between RPCs and the precipitation at grid points. Shaded areas are statistically significant at a 99% confidence level. Significant positive areas are darkly shaded and negative are lightly shaded.

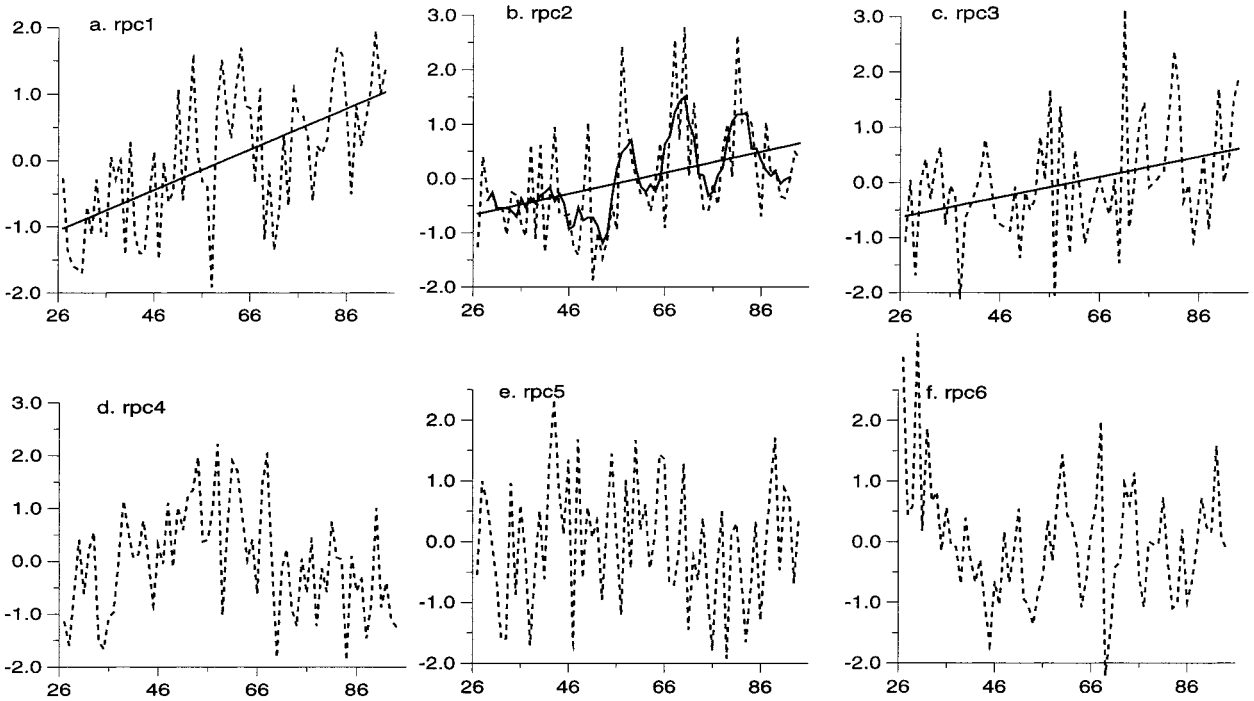

FIG. 7. Time series of the six RPCs (dashed lines), trends (solid lines), and the 5-yr moving averages (solid line).

Caspian Sea (Fig. 6c). The fourth REOF (REOF4) describes precipitation variation over southern-central Siberia, surrounding Lake Baikal (Fig. 6d). The fifth and sixth REOFs (REOF5 and REOF6) depict precipitation variations over the southwestern part of the study region and southwestern Siberia, respectively (Figs. 6e and 6f).

The time series of these six RPCs are plotted in Fig. 7. The first three RPCs show positive trends, and decadal variability is evident in RPC2 and RPC6. Least square trend lines are drawn over the first three RPCs and a 5-yr moving average line is overlaid on RPC2 in Fig. 7.

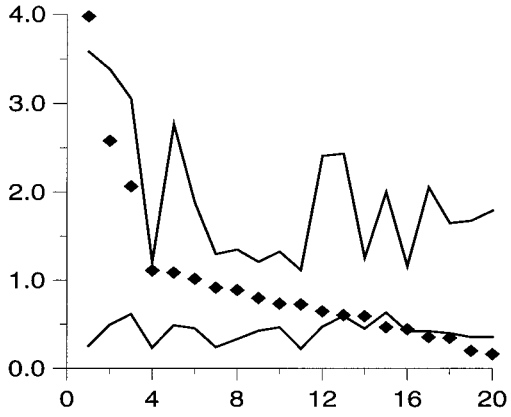

FIG. 8. Eigenvalue order (T-EOFs) of RPC2 and the 97.5 and 2.5 percentiles (solid lines) produced from 10 000 surrogate time series of red noises generated on the basis of the simple null hypothesis with some unknown noise parameters according to the formulation of Allen and Smith (1996). The first eigenvalue represents a trend component and explains more variance than expected null hypothesis.

To reveal dominant oscillation timescales by using SSA on each RPC, it is necessary to test any significant oscillations against colored noise by using a window length of 20. Given the short time series (68 yr it is hardly feasible to reveal any oscillations longer than 20 yr. Thus, the author only concentrates on oscillations shorter than 20 yr and any oscillations longer than 20 yr are considered to be part of the trend component. Trend component appears in the first T-PC of each of the first two RPCs and is found to be statistically significant at a 95% confidence level based on simple null hypothesis with some unknown noise parameters (section 4c in Allen and Smith 1996). The modified estimator proposed by Allen and Smith (1996) is used in this simple null hypothesis test. The eigenvalue rank of RPC2 and the 97.5 and 2.5 percentiles from 10 000 Monte Carlo simulations testing the simple null hypothesis with some unknown parameters are plotted in Fig. 8. The trend component (first T-PC) is above the 97% confidence level and the estimated single or more excursions above the 98.5 percentile is 8%.

Two T-PCs from RPC3 representing an oscillation of about 3 yr are also above the 97.5 percentile of the 10 000 Monte Carlo red-noise simulations. The probability of three or more excursions of the T-PC of RPC3 (these two T-PCs plus the first T-PC that represents low-frequency component) above the 97.5 percentile is 5.5% as calculated using the two-pass Monte Carlo approach (section 4b in Allen and Smith 1996). RPC4 also has two significant T-PCs representing a 4–5-yr oscillation. The probability of three

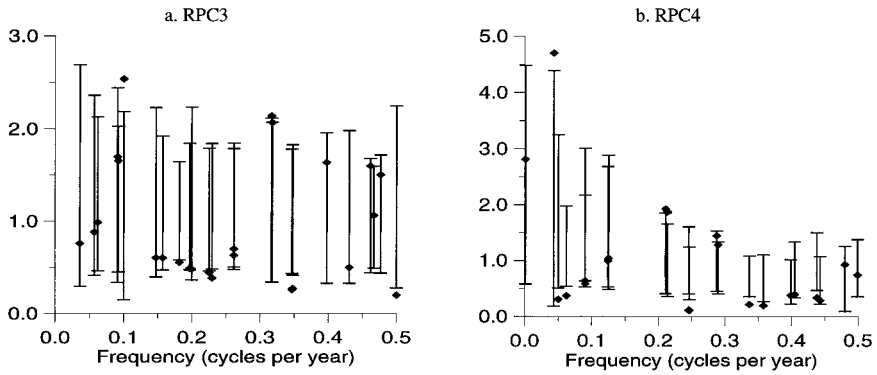

FIG. 9. Eigenspectra of (a) RPC3 and (b) RPC4 and the 97.5 and 2.5 percentiles produced from 10 000 surrogate time series of red noises generated on the basis of the simple null hypothesis with some unknown noise parameters according to the formulation of Allen and Smith (1996). The *x* axis represents frequency associated with eigenvalues (cycles per year). The *y* axis shows the power of eigenvalues.

or more excursions (these two T-PCs and the other low-frequency component) above the 97.5 percentile is also 5.5%. The spectrums of RPC3 and RPC4 and the 97.5 and 5.5 percentiles of red noises are shown in Fig. 9.

The composite null hypothesis test of the trend component of RPC2 plus red noises with some unknown noise parameters (section 4d in Allen and Smith 1996) suggests that two T-PCs representing a quasi-decadal oscillation component are significant above the 95% confidence level. The results of the test on composite null hypothesis of AR(1) noise plus the trend component of RPC2 is shown in Fig. 10. The two T-PCs corresponding to a quasi-decadal variation are above and very close to the 97.5 percentile, respectively. The probability of two or more excursions above the 97.5 percentile is estimated at about 15.7%. Given the evidence of similar timescale oscillation found in snow depth data over the same region (Ye 2000), the author takes this oscillation as a signal even though the significance level is not very high.

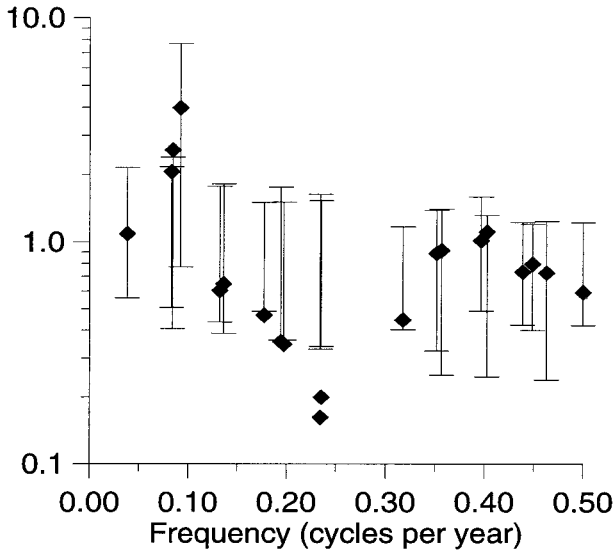

FIG. 10. Testing RPC2 against the composite null hypothesis of AR(1) plus trend component. The error bars are the 97.5 and 2.5 percentiles from 10 000 Monte Carlo simulations of red noises plus trend with some unknown noise parameters. The *x* axis represents frequency associated with eigenvalues (cycles per year). The *y* axis shows the power of eigenvalues.

After testing the statistical significance of the oscillation characteristics, SSA is applied to RPC2, RPC3, and RPC4 by using a window length of 13 yr. The 13-yr window length is chosen because it is longer than the significant oscillation time period yet it reduces the length of time in both ends of the RCs that may have phase shift. The algorithm used in SSA is adopted from Vautard and Ghil (1989) and the reconstruction method follows Vautard et al. (1992) who suggested no phase shift in the RCs if they came from oscillation pairs. The results are summarized in Table 2. In addition to a low-frequency component in each RPC, the second and third T-PC from SSA on RPC2 forms an oscillation pair representing an 11.8-yr oscillation. The sixth and seventh T-PC of RPC3 represent an oscillation pair with a period of 2.5 yr. The second and third T-PC of RPC4 consist of an oscillation pair of 4.75 yr. Each of these pairs qualifies by the two criteria listed in section 2b to be an oscillation pair.

The three reconstructed oscillation components of 2.5, 4.75, and 11.8 yr plus the significant low-frequency component along with the corresponding RPCs are plotted in Fig. 11 for visual examination. The reconstructed 11.8-yr oscillation component shows an increased amplitude and a more evident oscillation behavior in later decades (Fig. 11a). This time series resembles the 5-yr smoothing line of RPC2 in Fig. 7b.

b. Connections to the Atlantic Ocean

The simultaneous correlation coefficients between each RC and time series of SSTs at grid points over the

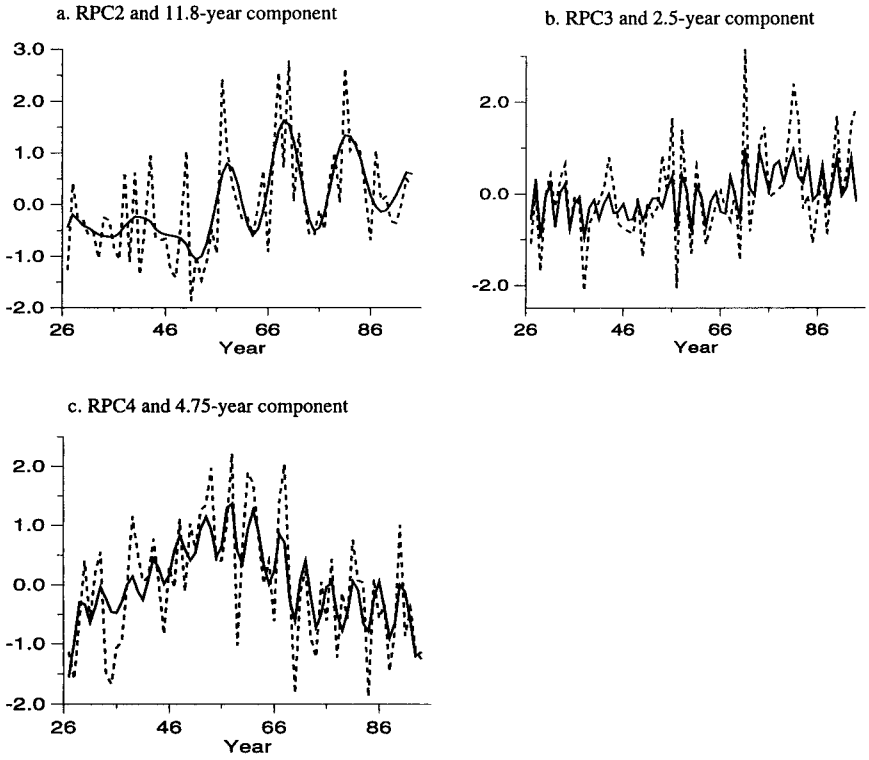

FIG. 11. The time series of RPCs (dashed lines) and the corresponding reconstructed oscillations added by the significant low-frequency component (solid lines).

Atlantic are calculated and compared with those using the corresponding RPC. Only RPC2 and its reconstructed quasi-decadal oscillation component have significant correlations with Atlantic SSTs. Also, the simultaneous cross-correlation maps between SSTs and the quasi-decadal component with two ends removed (26 yr total) and without two ends removed are calculated and compared. The resulting correlation coefficients patterns are very similar between those with and without the removal of the two ends. According to Vautard et al.'s (1992) suggestion of no phase shift if they are from an oscillation pair, and similar correlation patterns revealed in SSTs, the author presents results using the entire 68-yr correlation analysis for the rest of the paper since the removal of two ends in RCs does not affect significant correlation patterns in all analyses.

As a result, the quasi-decadal oscillation component of about 11.8 yr is more strongly correlated with Atlantic SSTs (Fig. 12a) than that using the corresponding RPC2. The decorrelation time of the correlations between RPC2 and Atlantic SSTs ranges from 1.05 to 1.55 suggesting that the independent sample size should be adjusted to a range of 47 to 65. The corresponding statistically significant correlations at a 95% confidence level range from 0.244 to 0.288. The resulting statistically significant areas adjusted for gridpoint sizes and autocorrelation is 19.7%, exceeding the Monte Carlo simulated rejection rate of 10.0%. This correlation coefficients pattern resembles the major SST variation pattern over the Atlantic revealed in many studies (e.g., Desser and Blackmon 1993; Livezey and Smith 1999; Peng and Mysak 1992; Xie and Tanimoto 1998).

Compared to those small significant correlation areas that correlated to RPC2 (not shown), the large significant areas and higher correlation coefficients revealed in this 11.8-yr component of RPC2 suggest that connections between RPC2 and the Atlantic Ocean are mostly evident at a quasi-decadal rather than an interannual timescale. This is consistent with quasi-decadal teleconnection characteristics between winter snow depth over European Russia and Atlantic SSTs (Ye 2000).

The cross-correlation maps with 1-yr lags between the quasi-decadal component and Atlantic SSTs are also produced. A similarly significant correlation pattern is found when Atlantic SSTs lead precipitation by one year (Fig. 12b). The correlation coefficients are slightly higher in northern latitude regions and statistically significant areas account for 21.2%. When precipitation leads SST by 1 yr, the correlation becomes very weak. This suggests that Atlantic SSTs persistently influence precipitation during the same and the next winter.

The cross-correlation maps using COAD's SST data produce very similar patterns suggesting that results are not sensitive to different SST datasets.

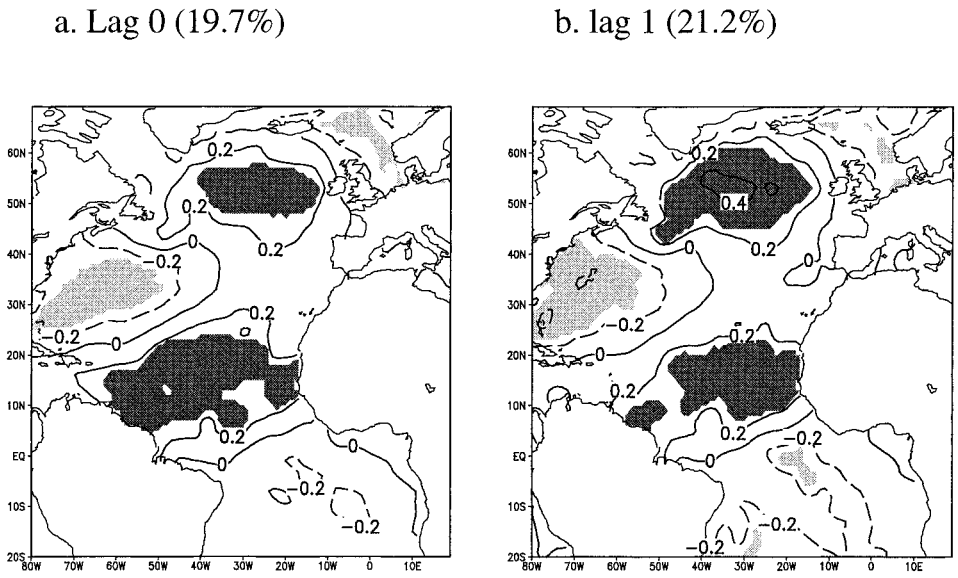

FIG. 12. Correlation coefficients between Atlantic SSTs and the 11.8 yr of RPC2: (a) simultaneous correlation and (b) SSTs lead 1 yr. Shaded areas are statistically significant at a 95% confidence level based on the adjusted sample size for autocorrelation. Negative values are depicted with dashed lines and are lightly shaded. The percentage of significant areas adjusted for gridpoint sizes are indicated in parentheses.

c. Connections to the Pacific Ocean

The 11.8-yr quasi-decadal oscillation is also found to be significantly associated with equatorial Pacific SSTs (Fig. 13a). The adjusted sample size for autocorrelation ranges from 44 to 65 and the corresponding 95% confidence correlation coefficients are 0.297 to 0.244. The resulting significant areas adjusted for gridpoint size account for 17.8% exceeding the rejection rate of 9.6% derived from 1000 Monte Carlo simulations for the Pacific Ocean. The significant correlation pattern remains when Pacific SSTs lag 1 yr behind (Fig. 13b). The lag relationship has a significant area of 18.9%. This suggests feedback of precipitation anomaly through atmospheric circulation to the equatorial Pacific SSTs at this quasi-decadal timescale.

The correlation coefficients map of Pacific SSTs relating to the 4.75-yr oscillation component of RPC4 shows that significant correlation areas are concentrated in the eastern Pacific, especially in the eastern tropical Pacific (Fig. 13c). The adjusted sample size for the correlation between Pacific SSTs and the 4.75-yr component of RPC4 ranges from 40 to 65 corresponding to the 95% confidence correlation coefficients of 0.244–0.312. The statistically significant areas adjusted for different gridpoint size are 26.0% exceeding the rejection rate of 9.6%. The statistically significant correlation area located over the eastern tropical Pacific coincides with the SST anomaly region under a typical El Niño condition. Since 4.75-yr variability falls within the range of the El Niño cycle, the precipitation over southern-central Siberia described by RPC4 is almost certainly teleconnected to El Niño activity. Few significant correlation coefficients are found when lag correlations are considered at this El Niño timescale.

These results stay the same when COAD's SSTs are used. This suggests the results of associations between precipitation and Pacific SSTs at quasi-decadal and El Niño timescales are not sensitive to different SST datasets.

d. Atmospheric circulation anomalies

Simultaneous correlation coefficients between time series of winter 700-mb heights at grid points and RPC2 and RPC4, and their reconstructed oscillation components are calculated. The significant correlation areas representing the circulation anomalies associated with the reconstructed oscillation components are generally consistent with those correlated to their corresponding RPCs. The correlation coefficients produced by using reconstructed oscillation components are slightly higher in some regions. The atmospheric anomaly patterns associated with the reconstructed oscillation components are displayed in Figs. 14 and 15. RPC2 and the associated 11.8-yr oscillation component are statistically significantly correlated with 700-mb height over the western Atlantic and eastern Pacific (Fig. 14) and all statistically significant areas lie north of 20°N. The opposite north–south correlation centering over the North Atlantic resembles the atmospheric west Atlantic pattern (WA; Barnston and Livezey 1987; Wallace and Gutzler 1981). This pattern is similar to the NAO except that the two centers are located toward the western Atlantic. Livezey and Smith (1999) revealed that an anomaly

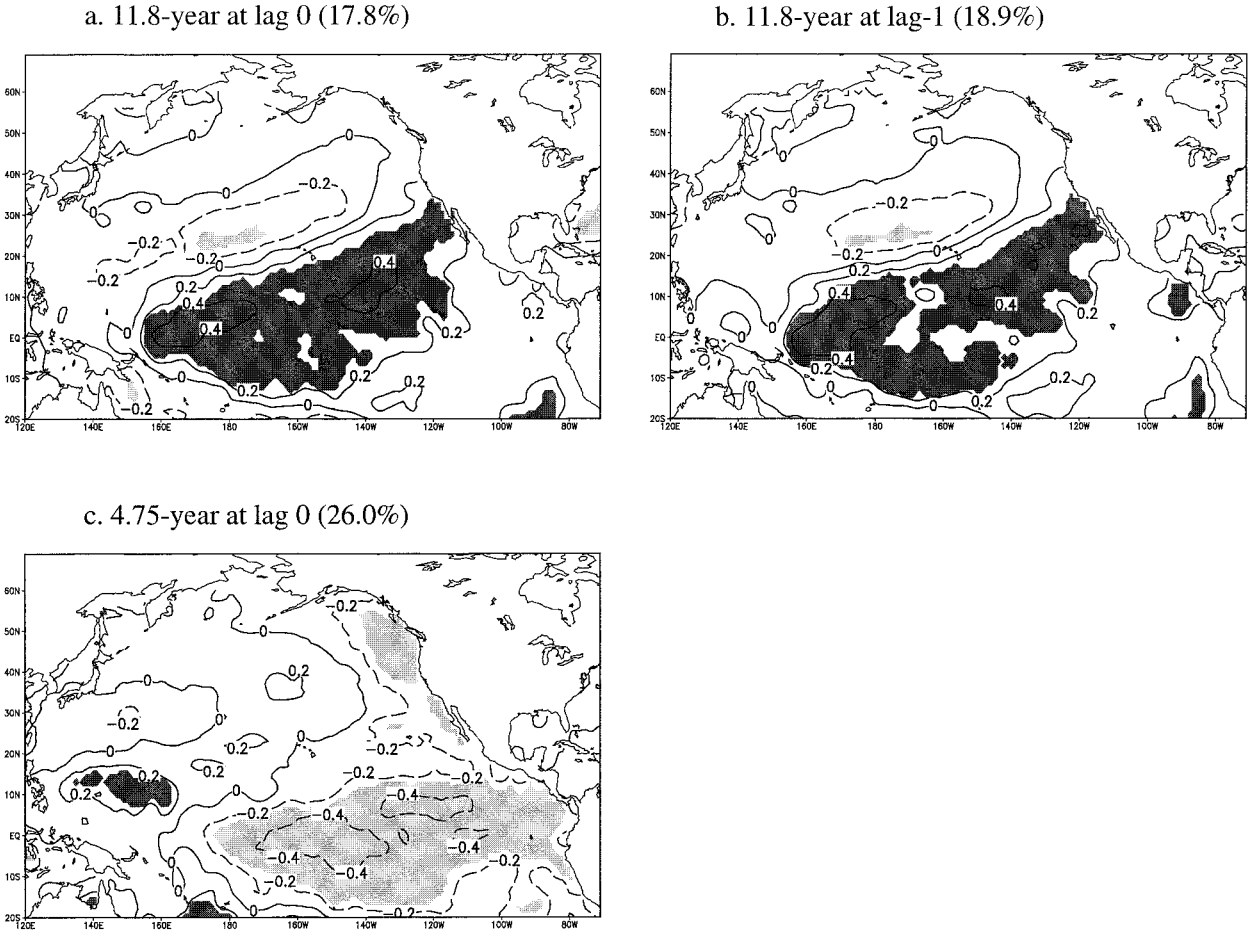

FIG. 13. The same as Fig. 12, except for the correlation coefficients between Pacific SSTs and the reconstructed oscillation component of (a) 11.8 yr of RPC2 at lag 0, (b) 11.8 yr of RPC2 with SST lag behind 1 yr, and (c) 4.75 yr of RPC4 at lag 0.

pattern of 700-mb geopotential heights similar to the pattern shown in Fig. 14 is closely associated with a pattern of SST anomalies that resembles the correlation pattern shown in Fig. 12a (see Fig. 2c in Livezey and Smith, 1999). They further revealed that such teleconnection has considerable variance at interdecadal timescales. This is consistent with the findings of the present study. The WA is found to be more strongly related to the Atlantic SST tendency than is the NAO (Wallace et al. 1990). This can be explained by the fact that the most effective atmospheric circulation in forcing SST anomalies should be the one that most strongly modulates surface wind speed (Wallace et al. 1990). This may be the reason that the teleconnection between SST and Eurasian precipitation is bridged through the WP instead of the NAO even though both patterns are part of the same decadal cycle related to North Atlantic SSTs as revealed by a recent modeling study (Häkkinen 2000). The negative anomaly center over the eastern Pacific shown in Fig. 14 corresponds to the connection of this variation mode over the Pacific Ocean.

To test the field significance of the associated atmospheric anomaly pattern, a rejection rate of 9.1% for significant correlations (at a 95% confidence level) over the area north of 20°N and 9.9% for the entire Northern Hemisphere 700-mb height are obtained through 1000 Monte Carlo simulations. The significant correlation areas adjusted for autocorrelation and different gridpoint sizes for the correlation pattern associated with the 11.8-yr oscillation is 17.9% over areas north of 20°N, greater than the rejection rate of 9.1% at the 95% confidence level.

When correlation coefficients are calculated with geopotential height leading precipitation by 1 yr, the pattern is very similar to the simultaneous relationship except that the northwestern Atlantic correlation center shifts eastward slightly and the center over the eastern Pacific covers a much smaller area (not shown). On the other hand, when geopotential height lags precipitation by 1 yr, the eastern Pacific center increases its significant area while the two centers over the Atlantic decrease their significant areas (not shown). The lag relationships between atmospheric circulation anomaly and precipita-

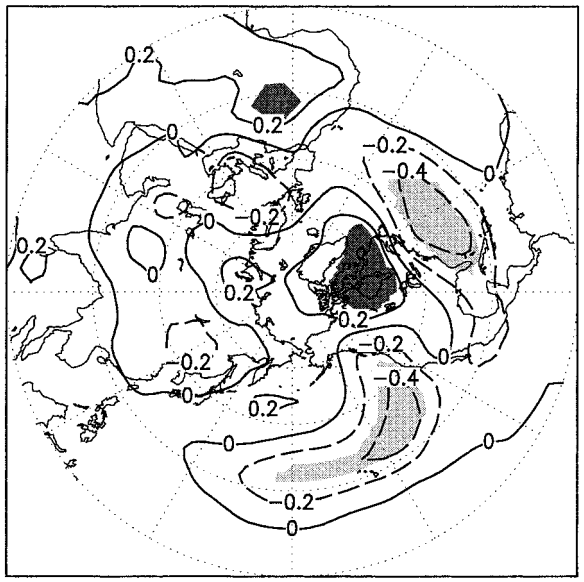

FIG. 14. Correlation coefficients between 700-mb heights and the reconstructed component of 11.8 yr of RPC2. Shaded areas are statistically significant at a 95% confidence level adjusted for the sample size due to autocorrelation. Negative values are depicted in dashed lines and are lightly shaded.

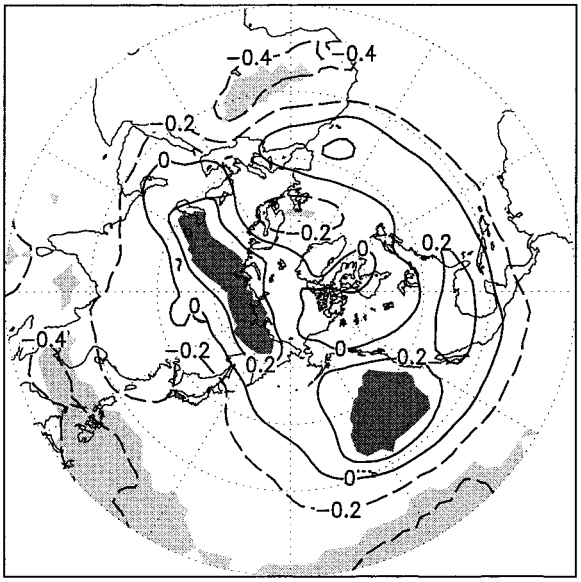

FIG. 15. The same as Fig. 14, except for 4.75-yr component of RPC4.

tion at this quasi-decadal timescale correspond well to those of SSTs over the Atlantic and Pacific Oceans.

The atmospheric circulation anomalies associated with the 4.75-yr variability are found over northern Eurasia, the eastern Pacific, and broad areas of the eastern and western tropical Pacific (Fig. 15). The total significant areas are 13.4% greater than the rejection rate (at a 95% confidence level) of 9.9% for the entire Northern Hemisphere and thus test the field significance of the atmospheric circulation pattern associated with this El Niño timescale precipitation variation.

The atmospheric anomaly center over the eastern Pacific coincides with one of the atmospheric anomalies associated with the ENSO mode of variability revealed by Livezey and Smith (1999). Also, this center is close to one of the active centers of the Pacific North American pattern (Barnston and Livezey 1987; Wallace and Gutzler 1981). It is likely that abnormal geopotential heights over the eastern Pacific coupled with eastern tropical Pacific SSTs are teleconnected to those over northern Eurasia at timescales of 4–5 yr and that the latter anomaly produces in-phase fluctuations in surface precipitation over southern-central Siberia. The physical mechanisms of the atmospheric anomaly associated with the identified oscillation modes in precipitation and SSTs need further investigation through theoretical and modeling research. This study only reveals statistical evidence of the associations observed in data records.

4. Conclusions

The temporal and spatial characteristics of winter precipitation variation over northern-central Eurasia are examined by using rotated PCA and SSA. Positive trends of about 0.4 mm yr^{-1} or 6% $decade^{-1}$ in precipitation are found over much of northern central Eurasia. In addition to these trends, precipitation oscillations of 2–3 yr, 4–5 yr, and 11–12 yr are found over southern European Russia, southern central Siberia, and central European Russia.

The precipitation variation of 2–3 yr (quasi biennial) and 4–5 yr (El Niño) found in this study are consistent with those found by Wang and Cho (1997) who used daily precipitation records for all seasons. The specific geographical regions associated with the two oscillations revealed in this winter study lie within the broader areas of significant oscillation defined by Wang and Cho (1997).

The quasi-periodical precipitation variations of 4–5 yr and 11–12 yr are statistically significantly associated with SSTs over the Pacific and Atlantic Oceans. The 4–5-yr precipitation variation is found teleconnected to eastern tropical SSTs and the El Niño region. El Niño–related atmospheric circulation anomalies over the eastern Pacific and northern Eurasia are responsible for this connection. The quasi-decadal precipitation variation of about 11–12 yr is associated with opposite latitudinal SST variations over the Atlantic Ocean, and SST anomalies over the equatorial North Pacific. The atmospheric WA pattern and an anomaly center over the eastern Pacific are associated with this quasi-decadal connection.

The revealed SST patterns that are associated with precipitation variations over northern-central Eurasia are not sensitive to different SST data produced by different reconstruction methods. The quasi-decadal and 4–5-yr precipitation variation over central European

Russia and southern central Russia and the teleconnection to Atlantic SSTs are consistent with those found in snow depth records for the time period of 1936–83 (Ye 2000). The common spatial and temporal variability characteristics revealed in these two studies using different observational records further suggest the true signatures inherent in winter precipitation and their teleconnections to SSTs.

A better understanding of teleconnections between SSTs and land surface climates will help to improve the prediction of surface climate (Barnston and Smith 1996). The mechanism for this type of teleconnection seems to be the persistent atmospheric circulation anomalies coupled with SSTs that exert their influences on distant land surface climates.

Modeling and observational studies have revealed close connections between atmospheric circulation and SST anomalies over the oceans (e.g., Chang et al. 1997; Davis 1976; Delworth and Stauffer 1993; Graham 1994; Häkkinen 2000; Kushnir and Lau 1992; Lanzante 1984; Lau 1997; Lau and Nath 1994; Namias 1963, 1969; Namias et al. 1988; Wallace 1993; Wallace et al. 1990). Atmosphere seems to be the primary driver for SST anomalies through surface wind, while the slow mode of SST variations and oceanic mixed layers likely contribute to persistent atmospheric anomaly patterns. Many of the atmospheric circulation patterns are directly associated with certain well-defined SST anomaly patterns over the Pacific and Atlantic Oceans. These atmospheric anomalies induce synergistic surface climate anomalies in widely separated geographic regions. This study reveals observational evidence of some well-known SST and atmospheric variation patterns and their associations with precipitation over high-latitude land areas. The statistical evidence discovered in this study complements modeling and theoretical studies focusing on the responses of regional climate variation to the external forcing of SSTs over the oceans.

Acknowledgments. The author appreciates the National Snow and Ice Data Centre for providing precipitation data, the British Atmospheric Data Center for providing GISST data, and NOAA–CIRES Climate Diagnostics Center for providing the COAD's SST dataset. Appreciation extends to the two anonymous reviewers' insightful comments on an earlier version of this paper that greatly improved its quality. The author also thanks Dr. David Legates, Dr. Cort Willmott, and Dr. Xuebin Zhang for discussions on gridpoint size adjustment and Argyl B. Houser for editing the final version of the manuscript. Finally, the author is very grateful to Dr. Eric Breitenberger for providing Matlab codes of SSA and Monte Carlo simulation in his Web site that saved a tremendous amount of computing time for the author. This research is supported by the Regional and Geography Program and the Climate Dynamics Program of the National Science Foundation.

REFERENCES

Allen, M. R., and L. A. Smith, 1996: Monte Carlo SSA: Detecting irregular oscillations in the presence of colored noise. *J. Climate,* **9,** 3373–3404.

Barnston, A. G., and R. E. Livezey, 1987: Classification, seasonality, and persistence of low-frequency atmospheric circulation patterns. *Mon. Wea. Rev.,* **115,** 1083–1126.

——, and T. M. Smith, 1996: Specification of prediction of global surface temperature and precipitation from global SST using CCA. *J. Climate,* **9,** 2660–2697.

Barrodale, I., and R. E. Erickson, 1980: Algorithms for least-squares linear prediction and maximum entropy spectral analysis. Part (I). Theory. *Geophysics,* **45,** 420–432.

Bitz, C. M., and D. S. Battisti, 1999: Interannual to decadal variability in climate and the glacier mass balance in Washington, Western Canada, and Alaska. *J. Climate,* **12,** 3181–3196.

Bradley, R. S., H. F. Diaz, J. K. Eischeid, P. D. Jones, P. M. Kelly, and C. M. Goodess, 1987: Precipitation fluctuations over Northern Hemisphere land areas since the mid-19th century. *Science,* **237,** 171–175.

Brown, R. D., 2000: Northern Hemisphere snow cover variability and change, 1915–97. *J. Climate,* **13,** 2339–2355.

Chang, P., L. Ji, and H. Li, 1997: A decadal climate variation in the tropical Atlantic Ocean from thermodynamic air–sea interactions. *Nature,* **386,** 516–518.

Chen, W. Y., 1982: Fluctuations in Northern Hemisphere 700-mb height field associated with the Southern Oscillation. *Mon. Wea. Rev.,* **110,** 808–823.

Cook, E. R., D. M. Meko, and C. W. Stockton, 1997: A new assessment of possible solar and lunar forcing of the bidecadal drought rhythm in the western United States. *J. Climate,* **10,** 1343–1356.

Currie, R. G., and D. P. O'Brien, 1992: Deterministic signals in USA precipitation records: II. *Int. J. Climatol.,* **12,** 281–304.

Dai, A., I. Y. Fung, and A. D. Genio, 1997: Surface observed global land precipitation variations during 1900–88. *J. Climate,* **10,** 2943–2962.

Davis, R. E., 1976: Predictability of sea surface temperature and sea level pressure anomalies over the North Pacific Ocean. *J. Phys. Oceanogr.,* **6,** 249–266.

Delworth, T. L., and R. J. Stouffer, 1993: Interdecadal variations of the thermohaline circulation in a coupled ocean–atmosphere model. *J. Climate,* **6,** 1993–2011.

Desser, C., and M. L. Blackmon, 1993: Surface climate variations over the North Atlantic Ocean during winter: 1900–1989. *J. Climate,* **6,** 1743–1953.

Dettinger, M. D., M. Ghil, and C. L. Keppenne, 1995: Interannual and interdecadal variability in United States surface-air temperatures, 1910–87. *Climatic Change,* **31,** 35–66.

Dickey, J. O., S. L. Marcus, and R. Hide, 1992: Global propagation of interannual fluctuations in atmospheric angular momentum. *Nature,* **357,** 484–488.

Eisheid, J. K., R. S. Bradley, and X. Shao, 1985: Secular climatic fluctuations in the Great Salt Lake basin. *Problems and Prospects for Predicting Great Salt Lake Levels,* P. Kay and H. F. Diaz, Eds., Center for Public Affairs and Administration, University of Utah, 111–122.

Elsner, J. B., and A. A. Tsonis, 1996: *Singular Spectrum Analysis: A New Tool in Time Series Analysis.* Plenum Press, 164 pp.

Fallot, J.-M., R. G. Barry, and D. Hoogstrate, 1997: Variations of mean cold season temperature precipitation and snow depths during the past 100 years in the former Soviet Union. *Hydrol. Sci. J.,* **42,** 301–327.

Folland, C. K., and D. E. Parker, 1995: Correction of instrumental biases in historical sea surface temperature data. *Quart. J. Roy. Meteor. Soc.,* **121,** 319–367.

——, T. Palmer, and D. E. Parker, 1986: Sahel rainfall and worldwide sea surface temperature, 1901–85. *Nature,* **320,** 602–607.

Fraedrich, K., C. Ziehmann, and F. Sielmann, 1995: Estimates of spatial degrees of freedom. *J. Climate,* **8,** 361–369.
Gershunov, A., T. P. Barnett, and D. R. Cayan, 1999: North Pacific interdecadal oscillation seen as factor in ENSO-related North American climate anomalies. *Eos, Trans. Amer. Geophys. Union,* **80,** 27–30.
Ghil, M., and K. Mo, 1991: Intraseasonal oscillations in the global atmosphere. Part I: Northern Hemisphere and Tropics. *J. Atmos. Sci.,* **48,** 752–779.
——, and R. Vautard, 1991: Interdecadal oscillations and the warming trend in global temperature time series. *Nature,* **350,** 324–327.
Graham, N. E., 1994: Decadale-scale climate variability in the tropical and North Pacific during the 1970s and 1980s: Observations and model results. *Climate Dyn.,* **10,** 135–162.
Groisman, P. Y., and D. R. Eastering, 1994: Variability and trends of total precipitation and snowfall over the United States and Canada. *J. Climate,* **7,** 184–205.
——, V. V. Koknaeva, T. A. Belodylova, and T. R. Karl, 1991: Overcoming biases of precipitation measurement: A history of the USSR experience. *Bull. Amer. Meteor. Soc.,* **72,** 1725–1733.
Guetter, A. K., and K. P. Georgakakos, 1993: River outflow of the conterminous United States, 1939–1988. *Bull. Amer. Meteor. Soc.,* **74,** 1873–1891.
Häkkinen, S., 2000: Decadal air–sea interaction in the North Atlantic based on observations and modeling results. *J. Climate,* **13,** 1195–1219.
Haston, L., and J. Michaelson, 1994: Long-term central coastal Californian precipitation variability and relationships to El Niño. *J. Climate,* **7,** 1373–1387.
Hurrell, J. W., 1995: Decadal trends in the North Atlantic oscillation: Regional temperatures and precipitation. *Science,* **269,** 676–679.
——, 1996: Influence of variations in extratropical wintertime teleconnections on Northern Hemisphere temperature. *Geophys. Res. Lett.,* **23,** 665–668.
——, and H. van Loon, 1997: Decadal variations in climate associated with the North Atlantic oscillation. *Climatic Change,* **36,** 301–326.
——, and K. E. Trenberth, 1999: Global sea surface temperature analyses: Multiple problems and their implications for climate analysis, modeling, and reanalysis. *Bull. Amer. Meteor. Soc.,* **80,** 2661–2678.
Jakowski, N., S. Schluter, and S. Heise, 2000: Analysis links Pacific decadal variability to drought and streamflow in United States. *Eos, Trans. Amer. Geophys. Union,* **80,** 621–625.
Kalnay, E., and Coauthors, 1996: The NCEP/NCAR 40-Year Reanalysis Project. *Bull. Amer. Meteor. Soc.,* **77,** 437–471.
Keppenne, C. L., and M. Ghil, 1992: Adaptive filtering and prediction of the Southern Oscillation index. *J. Geophys. Res.,* **97,** 20 449–20 454.
Kushnir, Y., 1994: Interdecadal variations in North Atlantic sea surface temperature and associated atmospheric conditions. *J. Climate,* **7,** 141–157.
——, and N.-C. Lau, 1992: The general circulation model response to a North Pacific SST anomaly: Dependence on timescale and pattern polarity. *J. Climate,* **5,** 271–283.
Lall, U., and M. Mann, 1995: The Great Salt Lake: A barometer of low-frequency climatic variability. *Water Resour. Res.,* **31**(10), 2503–2515.
Lanzante, J. R., 1984: A rotated eigenanalysis of the correlation between 700-mb heights and sea surface temperatures in the Pacific and Atlantic. *Mon. Wea. Rev.,* **112,** 2270–2280.
Latif, M., and T. P. Barnett, 1996: Decadal climate variability over the North Pacific and North America: Dynamics and predictability. *J. Climate,* **9,** 2406–2434.
——, R. Kleeman, and C. Eckert, 1997: Greenhouse warming, decadal variability, or El Niño? An attempt to understand the anomalous 1990s. *J. Climate,* **10,** 2221–2239.
Lau, N.-C., 1997: Interactions between global SST anomalies and the midlatitude atmospheric circulation. *Bull. Amer. Meteor. Soc.,* **78,** 21–33.
——, and M. J. Nath, 1994: A modeling study if the relative roles of tropical and extratropical SST anomalies in the variability of the global atmosphere–ocean system. *J. Climate,* **7,** 1184–1207.
Liang, X.-Z., A. N. Samel, and W.-C. Wang, 1995: Observed and GCM simulated decadal variability of monsoon rainfall in east China. *Climate Dyn.,* **11,** 103–114.
Livezey, R. E., and W. Y. Chen, 1983: Statistical field significance and its determination by Monte Carlo techniques. *Mon. Wea. Rev.,* **111,** 46–59.
——, and T. M. Smith, 1999: Covariability of aspects of North American climate with global sea surface temperatures on interannual to interdecadal timescales. *J. Climate,* **12,** 289–302.
Mann, M. E., and J. Park, 1994: Global-scale modes of surface temperature variability on interannual to century timescales. *J. Geophys. Res.,* **99,** 25 819–25 833.
——, and ——, 1996: Joint spatiotemporal modes of surface temperature and sea level pressure variability in the Northern Hemisphere during the last century. *J. Climate,* **9,** 2137–2162.
——, U. Lall, and B. Saltzman, 1995: Decadal-to-centennial-scale climate variability: Insights into the rise and fall of the Great Salt Lake. *Geophys. Res. Lett.,* **22,** 937–940.
Moses, T., G. N. Kiladis, H. F. Diaz, and R. G. Barry, 1987: Characteristics and frequency of reversals in mean sea level pressure in the North Atlantic sector and their relationship to long-term temperature trends. *J. Climatol.,* **7,** 13–30.
Namias, J., 1963: Large-scale air–sea interactions over the North Pacific from summer 1962 through the subsequent winter. *J. Geophys. Res.,* **68,** 6171–6186.
——, 1969: Seasonal interactions between the North Pacific Ocean and the atmosphere during the 1960s. *Mon. Wea. Rev.,* **97,** 173–192.
——, X. Yuan, and D. R. Cayan, 1988: Persistence of North Pacific sea surface temperature and atmospheric flow patterns. *J. Climate,* **1,** 682–703.
North, G. R., L. B. Thomas, and R. F. Cahalan, 1982: Sampling error in the estimation of empirical orthogonal functions. *Mon. Wea. Rev.,* **110,** 699–706.
Parker, D. E., C. K. Folland, and M. Jackson, 1995: Marine surface temperature: Observed variations and data requirements. *Climatic Change,* **31,** 559–600.
Peng, S., and L. A. Mysak, 1993: A teleconnection study of interannual sea surface temperature fluctuation in the northern North Atlantic and precipitation and runoff over western Siberia. *J. Climate,* **6,** 876–885.
Pierce, D., T. P. Barnett, and M. Latif, 2000: Connections between the Pacific Ocean Tropics and midlatitudes on decadal timescales. *J. Climate,* **13,** 1173–1194.
Plaut, G., and R. Vautard, 1994: Spells of low-frequency oscillations and weather regimes in the Northern Hemisphere. *J. Atmos. Sci.,* **51,** 210–236.
Reed, R. J., W. J. Campbell, L. A. Rasmussen, and D. G. Rogers, 1961: Evidence of downward-propogating annual wind reversal in the equatorial stratosphere. *J. Geophys. Res.,* **66,** 813–818.
Reverdin, G., D. Cayan, and Y. Kushnir, 1997: Decadal variability of hydrography in the upper northern North Atlantic in 1948–1990. *J. Geophys. Res.,* **102**(C4), 8505–8531.
Richman, M. B., 1986: Rotation of principal components. *J. Climatol.,* **6,** 293–335.
——, 1987: Rotation of principal components: A reply. *J. Climatol.,* **7,** 511–520.
Rogers, J. C., 1997: North Atlantic storm track variability and its association to North Atlantic oscillation and climate variability of northern Europe. *J. Climate,* **10,** 1635–1647.
Ropelewski, C. F., and M. S. Helpert, 1987: Global and regional scale precipitation patterns associated with the El Niño/Southern Oscillation. *Mon. Wea. Rev.,* **115,** 1606–1626.
Sathiyamoorthy, V., and K. Mohanakumar, 2000: Characteristics of tropospheric biennial oscillation and its possible association with the stratospheric QBO. *Geophys. Res. Lett.,* **27,** 669–672.
Shen, S., and K.-M. Lau, 1995: Biennial oscillation associated with

the East Asian summer monsoon and tropical sea surface temperatures. *J. Meteor. Soc. Japan*, **73,** 105–124.
Smith, T. M., R. W. Reynolds, R. E. Livezey, and D. C. Stokes, 1996: Reconstruction of historical sea surface temperatures using empirical orthogonal functions. *J. Climate*, **9,** 1403–1420.
Ting, M., and H. Wang, 1997: Summertime U.S. precipitation variability and its relation to Pacific sea surface temperature. *J. Climate*, **10,** 1853–1873.
Trenberth, K. E., and J. G. Olson, 1988: An evaluation and intercomparison of global analyses from the National Meteorological Center and the European Centre for Medium Range Weather Forecasts. *Bull. Amer. Meteor. Soc.*, **69,** 1047–1057.
Vautard, R., and M. Ghil, 1989: Singular spectrum analysis in nonlinear dynamics with applications to paleoclimatic time series. *Physica D*, **35,** 395–424.
——, P. Yiou, and M. Ghil, 1992: Singular-spectrum analysis: A toolkit for short, noisy chaotic signals. *Physica D*, **58,** 95–126.
Veryard, R. G., and R. A. Ebdon, 1961: Fluctuation in tropical stratospheric winds. *Meteor. Mag.*, **90,** 125–143.
von Storch, H., and A. Navara, Eds., 1999: *Analysis of Climate Variability: Applications of Statistical Techniques.* 2d ed. Springer, 342 pp.
——, and F. W. Zwiers, 1999: *Statistical Analysis in Climate Research.* Cambridge University Press, 484 pp.
Wallace, J. M., 1993: Forced and free variability in the climate record. *Proc. Workshop on Decade-to-Century Time Scales of Climate Variability*, Irvine, CA, National Research Council, Board on Atmospheric Science and Climate, National Academy of Sciences.
——, and D. S. Gutzler, 1981: Teleconnections in the geopotential height field during the Northern Hemisphere winter. *Mon. Wea. Rev.*, **109,** 784–812.
——, C. Smith, and Q. Jiang, 1990: Spatial patterns of atmosphere–ocean interaction in the northern winter. *J. Climate*, **3,** 990–998.
——, ——, and C. S. Bretherton, 1992: Singular value decomposition of wintertime sea surface temperature and 500-mb height anomalies. *J. Climate*, **5,** 561–576.
——, Y. Zhang, and J. A. Renwick, 1995: Dynamics contribution to hemispheric mean temperature trends. *Science*, **270,** 780–783.
Wang, X. L., and H. Cho, 1997: Spatial–temporal structures of trend and oscillatory variability of precipitation over Northern Eurasia. *J. Climate*, **10,** 2285–2298.
Willmott, C. J., C. M. Rowe, and W. D. Philpot, 1985: Small-scale climate maps: A sensitivity analysis of some common assumptions associated with the grid-point interpolation and contouring. *Amer. Cartographer*, **12,** 5–16.
Xie, S.-P., and Y. Tanimoto, 1998: A pan-Atlantic decadal climate oscillation. *Geophys. Res. Lett.*, **25,** 2185–2188.
Yamagata, T., and Y. Masumoto, 1992: Interdecadal natural climate variability in the western Pacific and its implication in global warming. *J. Meteor. Soc. Japan*, **70,** 37–175.
Yatagai, A., and T. Yasunari, 1994: Trends and decadal-scale fluctuations of surface air temperature and precipitation over China and Mongolia during the recent 40-year period (1951–1990). *J. Meteor. Soc. Japan*, **72,** 937–957.
Ye, H., 2000: Decadal variability of Russian winter snow accumulation and its associations with Atlantic sea surface temperature anomalies. *Int. J. Climatol.*, **20,** 1709–1728.
——, H. Cho, and P. E. Gustafson, 1998: The changes in Russian winter snow accumulation during 1936–83 and its spatial patterns. *J. Climate*, **11,** 856–863.
Zhang, X., J. Sheng, and A. Shabbar, 1998: Modes of interannual and interdecadal variability of Pacific SST. *J. Climate*, **11,** 2556–2569.
Zhang, Y., J. M. Wallace, and D. S. Battisti, 1997: ENSO-like interdecadal variability: 1900–93. *J. Climate*, **10,** 1004–1020.